

# Van Hove singularities in the density of states of a chaotic dynamical system

**Bryn Davies**

Department of Mathematics, Imperial College London, London, UK

E-mail: bryn.davies@imperial.ac.uk

**Abstract.** The statistics of a chaotic recursion relation can be predicted by constructing an associated sequence of periodic elliptic operators. For such operators, the density of states is well understood, can be computed straightforwardly and explicit formulas can often be derived. The example studied here is a non-linear recursion relation which can be related to a sequence of periodic operators generated by a Fibonacci tiling rule. This link is used to derive an explicit formula for the limiting distribution of orbits of the non-linear recursion relation. This distribution contains characteristic features of the associated operators' densities of states, such as Van Hove singularities near to critical values.

**Keywords.** density of states, dynamical system, chaos, Fibonacci tiling, non-linear recursion relation, limiting distribution

**Mathematics Subject Classification.** 37A50, 34B05, 34L05, 35J25

## 1. Introduction

Non-linearities in dynamical systems can make it difficult to predict the long-time behaviour of a given orbit from its initial conditions. Indeed, such systems can exhibit chaotic behaviour including extreme sensitivity on initial conditions. However, the collective behaviour of many different orbits of even the most chaotic systems is often possible to capture in a statistical sense. Thus, a typical question to ask is if the initial conditions are chosen at random from a given distribution, what will be the distribution after the system has been allowed to evolve for a given period?

Using probabilistic methods, it is often possible to make precise and accurate statements about the likelihood of a future state in a chaotic system. The breadth of stochastic methods for non-linear and chaotic systems are surveyed in [28]. Many of the most popular and successful approaches are based on computing the density of states through exploiting Ergodic properties and finding invariant measures [43]. It is also possible to understand a system's statistics by reformulating the problem in terms of random matrix theory [11, 19].

Useful results for understanding the long-time behaviour of orbits can take many different forms. One useful piece of information is understanding if and when a

sequence will diverge. For example, for the non-linear recursion relation that defines the Mandelbrot set (*i.e.*  $x_{n+1} = x_n^2 + x_1$ ), it is straightforward to show that if  $|x_n| > 2$  for any  $n$ , then the sequence is guaranteed to diverge (the circle of radius 2 in the complex plane is a “divergence horizon”) [30]. For orbits that remain bounded, it is useful to know how elements of the sequence are likely to be distributed. For example, for the chaotic logistic map (*i.e.*  $x_{n+1} = 4x_n(1 - x_n)$ ) it is known that the long-time distribution of states within the interval  $(0, 1)$  is given by a beta distribution with parameters  $a = 0.5$  and  $b = 0.5$  (*i.e.*  $D(x) = \pi^{-1}x^{-1/2}(1 - x)^{-1/2}$ ) [22]. This follows from the fact that this distribution is an invariant measure for the logistic map (which is an example of a general result concerning invariant measures for dynamical systems with attractors).

There is a well-known link between dynamical systems and spectral properties of one-dimensional differential operators. This link has underpinned several significant breakthroughs. For example, several important results in the spectral theory of one-dimensional operators with quasi-periodic coefficients are based on reformulating the problem in the language of dynamical systems, *e.g.* [4, 37, 38]. Indeed, this is fundamentally the reason that the spectral theory of quasi-periodic operators is so much more developed in one dimension than for multi-dimensional systems (for which little theory exists). Similarly, approaches for one-dimensional random systems often use ideas with analogues in dynamical systems theory, such as the use of Lyapunov functions to characterise decay rates and mean free paths, see *e.g.* [5, 7, 8, 34].

This work considers a non-linear recursion relation which can be related to a sequence of periodic operators generated by a Fibonacci tiling rule. The recursion relation is

$$x_{n+1} = x_n x_{n-1} - x_{n-2}, \tag{1.1}$$

where the initial conditions  $x_0, x_1$  and  $x_2$  are taken to be real numbers. The main setting considered in this work is where  $x_0$  and  $x_1$  are independent random variables and  $x_2$  is chosen to depend on  $x_0$  and  $x_1$ . Under particular choices of  $x_2$ , an associated sequence of periodic operators can be constructed using a Fibonacci tiling rule. This connection was first realised by [23] and leads to a sequence of one-dimensional periodic elliptic operators with coefficients given by a Fibonacci tiling rule. Related materials have enjoyed a resurgence in the literature recently, with the development of quasi-periodic metamaterials [10, 12, 20, 21, 42].

This recursion relation (1.1) is conservative but exhibits chaotic behaviour in the sense of sensitive dependence on initial conditions. It is possible to characterise orbits of (1.1) that diverge through a version of a “divergence horizon” at the edges of the interval  $[-2, 2]$  (through a generalisation of existing results from [10]). The main question studied in this work is to understand the limiting distribution of orbits of (1.1) that remain bounded (when the distribution of the initial conditions is known). The approach taken here is to exploit the associated sequence of periodic elliptic operators, for which the spectral properties are well understood [27]. This includes the density of states associated to a given spectrum, which is used here to derive an explicit formula for the limiting distribution of orbits of the non-linear recursion relation. This distribution

contains characteristic features of the associated operators' densities of states, such as Van Hove singularities [41] near to the edges of the critical interval  $[-2, 2]$ .

This paper will begin by exploring the basic properties of the recursion relation (1.1) in Section 2 and summarising the requisite spectral theory for periodic elliptic operators in Section 3. In Section 4, the associated sequence of Fibonacci-generated operators will be constructed. Finally, the main result will be a formula for the density of states of the recursion relation (1.1), which is computed using the associated operators and is presented in Section 5.

## 2. Problem setting and preliminaries

### 2.1. Basic properties

The first known detailed study of the behaviour of the recursion relation (1.1) was performed by [23] as part of a seminal study of the spectrum of a Schrödinger equation with quasiperiodic potential (the same link that will be exploited here, in the subsequent analysis). It is conservative in the sense that if it is framed as a three-dimensional map  $\mathbf{x}_{n+1} = f(\mathbf{x}_n)$  where  $f : \mathbb{R}^3 \rightarrow \mathbb{R}^3$  is given by

$$f(x, y, z) := (xy - z, x, y), \tag{2.1}$$

then its Jacobian  $J$  is always such that  $\det(J) = -1$ . The recursion relation (1.1) also has a known invariant. It was discovered by [24] that the quantity

$$I = x^2 + y^2 + z^2 - xyz, \tag{2.2}$$

is invariant under the map (2.1). This invariant has played an important role in historic studies of the properties of (1.1) as orbits are constrained to the two-dimensional manifold described by the level sets of  $I$  [24, 32].

Some exemplar orbits of (1.1) are shown in Figure 1. In each case, the initial values  $x_0$ ,  $x_1$  and  $x_2$  are chosen to lie within the interval  $[-2, 2]$ . It is immediately apparent that the behaviour typically takes one of three forms. In some cases, the orbit appears to stay bounded, fluctuating erratically within the interval  $[-2, 2]$ , as shown in Figures 1(a)–(c). However, for some initial conditions the orbit escapes the interval  $[-2, 2]$  and then diverges quickly, as shown in Figures 1(d)–(e). Finally, there also exist periodic orbits. One is depicted in Figure 1(f), which is an example of the 6-periodic orbits that will occur if any two of the three initial values are zero. Notice that the repeating non-zero value can be arbitrarily large (in particular, it can be either inside or outside of the critical interval  $[-2, 2]$ ).

Characterising whether the recursion relation (1.1) diverges for a given set of initial conditions has been one of the main questions considered in the literature. The behaviour observed in Figure 1 might suggest behaviour similar to the recursion relation used to define the Mandelbrot set (*i.e.*  $x_{n+1} = x_n^2 + x_0$ ) whereby once the orbit leaves the critical interval  $\{|x_n| \leq 2\}$  it is guaranteed to diverge. However, the existence of

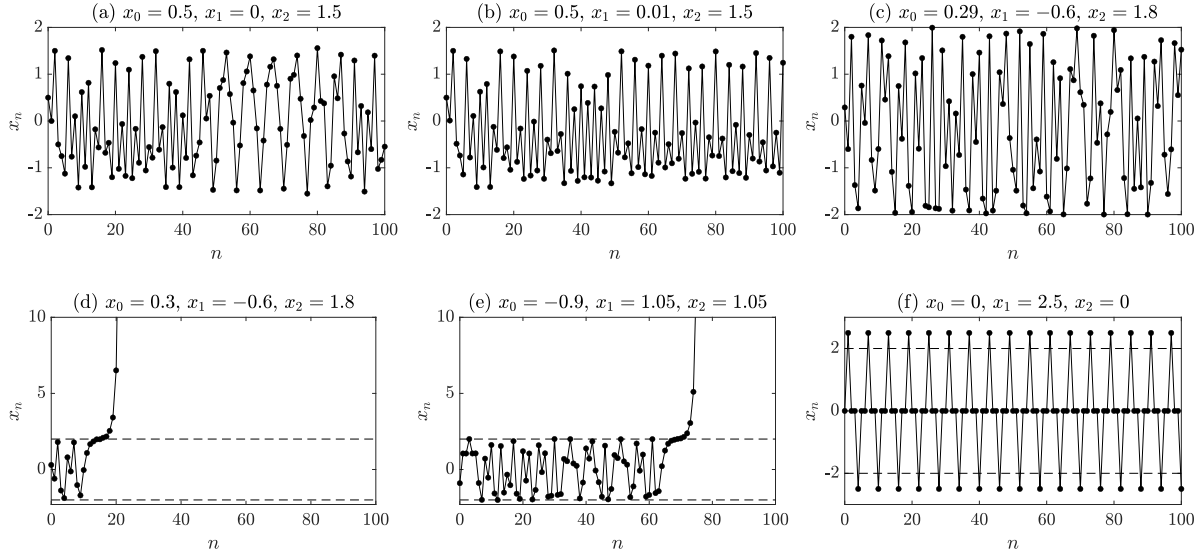


Figure 1: Exemplar orbits of the recursion relation (1.1) for different initial conditions. Dashed lines indicate the critical threshold  $|x_n| = 2$ . Examples (a)–(c) are bounded by this threshold (for the 100 terms shown), while (d) and (e) diverge after exceeding it. (f) shows an example of a periodic orbit that exceeds this threshold every third term.

periodic orbits taking arbitrarily large values (as in Figure 1(f)) shows that no such result is possible. Instead, the following result was proved in [10], showing that if an orbit is outside of the interval  $[-2, 2]$  and it has three successive terms that are growing, then it is guaranteed to diverge. Since the version of this result proved in [10, Theorem 3.1] is slightly weaker, a modification of the proof is included here for completeness.

**Lemma 1.** *Suppose that  $\{x_n : n \in \mathbb{Z}^{\geq 0}\}$  satisfies the recursion relation (1.1). If there exists some  $N \in \mathbb{Z}^{\geq 0}$  such that*

$$2 < |x_N|, \quad |x_N| < |x_{N+1}|, \quad |x_{N+1}| < |x_{N+2}|,$$

then  $|x_n| > 2$  for all  $n \geq N$  and  $|x_n| \rightarrow \infty$  as  $n \rightarrow \infty$ .

*Proof.* It is easy to see that

$$|x_{N+3}| \geq |x_{N+2}||x_{N+1}| - |x_N| \geq |x_{N+2}||x_N| - |x_N| = |x_{N+2}|(|x_N| - 1) + (|x_{N+2}| - |x_N|).$$

By hypothesis,  $|x_{N+2}| > |x_N|$  meaning that  $|x_{N+3}| > |x_{N+2}|(|x_N| - 1)$ , where  $(|x_N| - 1) > 1$ . Proceeding by induction, it can be shown that

$$|x_{N+2+n}| > |x_{N+2}|(|x_N| - 1)^n, \quad (2.3)$$

for all  $n \in \mathbb{Z}^{> 0}$ , from which it is clear that  $|x_n| \rightarrow \infty$  as  $n \rightarrow \infty$ .  $\square$

Under suitable parametrisation of the initial conditions (in the spirit of the condition that will be introduced to fix the dependence of  $x_2$  on  $x_0$  and  $x_1$  in (2.5)

here), the set of initial conditions for which the recursion relation (1.1) remains within the bounded interval  $[-2, 2]$  is known to be a Cantor set (*i.e.* a closed set with no isolated points and whose complement is dense) [24, 39]. Further, this set has zero Lebesgue measure [39] and displays the self-similar properties typical of fractals [23, 32].

While Lemma 1 characterises the divergence that can occur when an orbit leaves the critical interval  $[-2, 2]$ , the question considered in this work is how states behave while they remain within this interval. From the bounded orbits shown in Figure 1, it is clear that this behaviour is erratic and exhibits the sensitive dependence on initial conditions typical of chaotic systems. However, is it possible to describe the overall distribution of states within this interval?

### 2.2. Distribution of states

A natural first question to ask is how the orbits of (1.1) are distributed on the interval  $[-2, 2]$  when the initial conditions  $x_0, x_1, x_2$  are chosen such that they are all independent of one another. For example, suppose they are generated at random satisfying uniform distributions on  $[-2, 2]$ . In this case, histograms showing the distribution of the orbits are given in Figure 2. Figure 2(a)–(c) show the distribution of  $x_3, x_4$  and  $x_5$  restricted to  $[-2, 2]$ , with each histogram showing the result of  $10^5$  independent realisations of the initial conditions. Then, Figure 2(d) shows what will be referred to here as the long-time distribution of the recursion relation: for each of the  $10^5$  realisations of the initial conditions, the first 200 iterations of the recursion relation are computed and all those falling within the interval  $[-2, 2]$  are plotted.

In this case, it is apparent that the long-time distribution of the orbits restricted to the interval  $[-2, 2]$  is described by the semicircle distribution with radius 2, given by

$$D(x) = \frac{1}{2\pi} \sqrt{4 - x^2}. \tag{2.4}$$

This distribution is indicated by the dashed line in Figure 2(d). The “rounded” nature of the distribution is already beginning to emerge from the distributions of the first few values, as depicted in Figure 2(a)–(c). The distribution of  $x_3 = x_2x_1 - x_0$  can be calculated explicitly, as given in Lemma 2 and indicated on Figure 2(a) by the dashed line. Then, subsequent elements of the sequence are increasingly concentrated around zero, such that the semicircle distribution (2.4) is recovered in the limit.

**Lemma 2.** *If  $X_0, X_1$  and  $X_2$  are independent random variables each drawn from a uniform distribution on the interval  $[-2, 2]$ , then the variable  $X_3 = X_2X_1 - X_0$  has the probability density function*

$$f_{X_3}(x) = \frac{x-2}{32} \log\left(\frac{2-x}{4}\right) - \frac{x+2}{32} \log\left(\frac{x+2}{4}\right) + \frac{1}{8},$$

for  $-2 \leq x \leq 2$ .

*Proof.* This follows from routine calculations for products and sums of random variables, the details of which are given in Appendix A. □

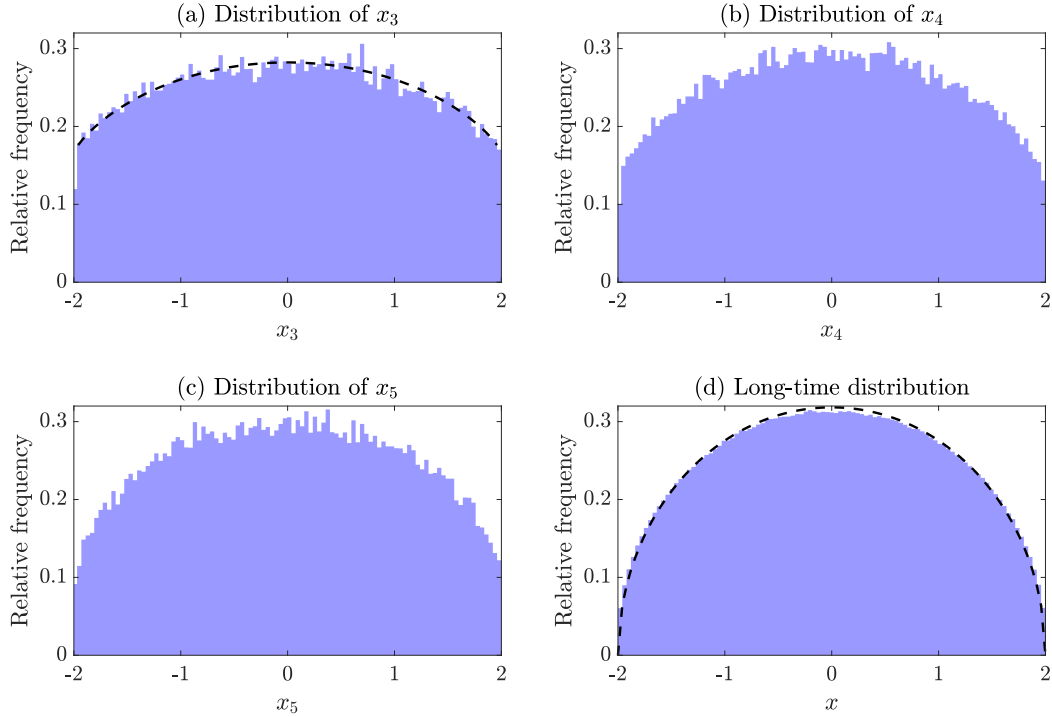


Figure 2: The distribution of states of the recursion relation (1.1) when the initial values  $x_0$ ,  $x_1$  and  $x_2$  are independent and uniformly distributed on  $[-2, 2]$ . The dashed lines in (a) and (d) show the distributions from Lemma 2 and (2.4), respectively. The long-time distribution contains the first 200 terms and  $10^5$  independent realisations of the initial conditions are used for each histogram.

The focus of this work, however, is the behaviour of the recursion relation when  $x_2$  is chosen to depend on  $x_1$  and  $x_0$ . In particular, defining the quantities  $\omega_0 = \arccos(x_0/2)$  and  $\omega_1 = \arccos(x_1/2)$ , the desired relation is that  $x_2$  is given by

$$x_2 = 2 \cos \omega_0 \cos \omega_1 - \left( \frac{\omega_0}{\omega_1} + \frac{\omega_1}{\omega_0} \right) \sin \omega_0 \sin \omega_1. \quad (2.5)$$

The motivation for this specific choice of relationship will become apparent in Section 4: it will allow for a sequence of periodic elliptic operators to be constructed whose spectra can be related to the elements in a given orbit of the recursion relation (1.1).

When  $x_2$  is chosen to depend on  $x_0$  and  $x_1$  according to (2.5), the distributions of the states of the recursion relation (1.1) are shown in Figure 3. Even calculating the distribution of  $x_2$  to describe the shape of Figure 3(a), analogous to Lemma 2 for the case of fully independent initial conditions, is less straightforward in this case, due to the intricate nature of the dependence (2.5). However, the crucial feature to observe is the clustering of values around  $-2$ , due to the corresponding clustering of values of the terms in (2.5) (this is explored in more detail in Appendix B).

The main feature that is apparent from Figure 3 is the tendency for states to cluster around the edges of the interval  $[-2, 2]$ . The long-time distribution, in Figure 3(d), shows

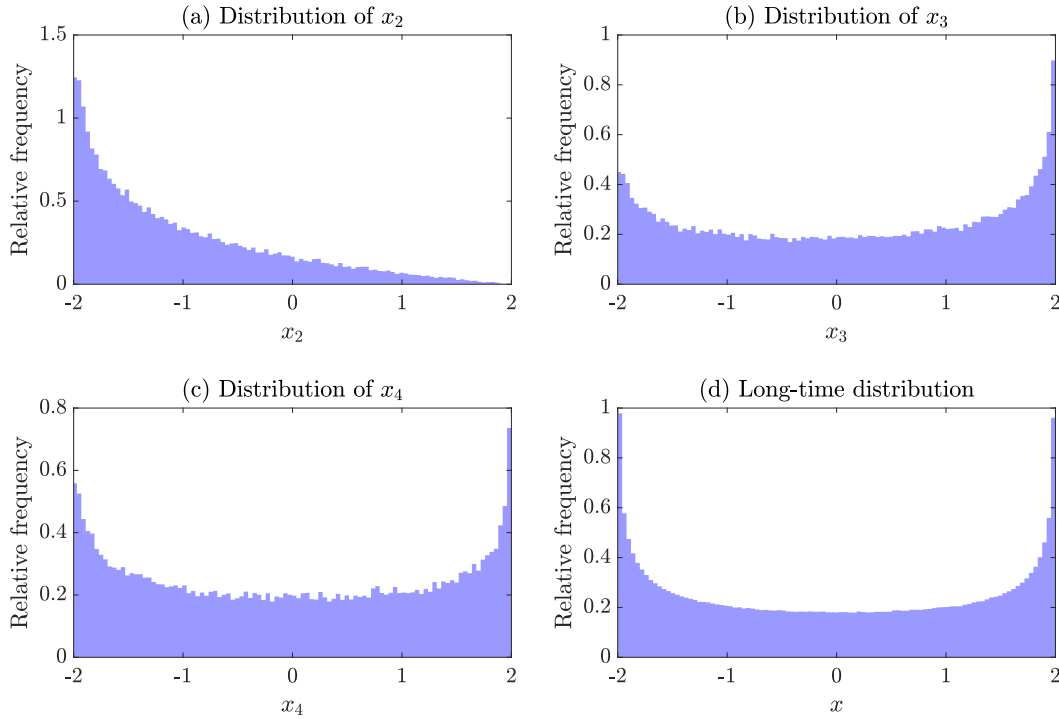


Figure 3: The distribution of states of the recursion relation (1.1) when the initial values  $x_0$  and  $x_1$  are independent and uniformly distributed on  $[-2, 2]$  and  $x_2$  is chosen to depend on  $x_0$  and  $x_1$  according to (2.5). The long-time distribution contains the first 200 terms and  $10^5$  independent realisations of the initial conditions are used in each histogram.

a symmetric distribution that appears to display singularities at  $x = \pm 2$ . The main goal of this work is to describe this distribution by exploiting links with the densities of states of a related sequence of periodic elliptic operators. Then, the singular nature of the distribution at  $x = \pm 2$  can be related to the well-known *Van Hove singularities* [41], which will be introduced in Section 3.2.

### 3. Spectral theory for periodic elliptic operators

Periodic elliptic operators are particularly convenient to work with as their spectra are composed of a countable series of continuous spectral bands. Further, the associated density of states (which, roughly speaking, describes how eigenvalues are distributed within these continuous bands) can be understood as a function of the slope of these bands. The main ideas of this theory are summarised below, for the particular case of ordinary differential operators. A more comprehensive review can be found in [27] and references therein.

### 3.1. Floquet theory for Hill operators

Consider the *Hill operator*, given by

$$\mathcal{H}_L = \frac{d^2}{dx^2} + V(x), \quad (3.1)$$

where  $V : \mathbb{R} \rightarrow \mathbb{R}$  is some potential function, which is supposed to be piecewise smooth (in fact, piecewise constant will be sufficient here) and  $L$ -periodic (*i.e.*  $V(x) = V(x+L)$  for any  $x \in \mathbb{R}$ ). The eigenvalue problem for  $\mathcal{H}_L$  that is of interest here is

$$\mathcal{H}_L u = \lambda u. \quad (3.2)$$

A key tool for understanding the solution space of (3.2) is the *monodromy matrix*. Given the basis functions  $\phi(x, \lambda)$  and  $\psi(x, \lambda)$ , which are defined as solutions to (3.2) satisfying the boundary conditions  $\phi(0, \lambda) = \partial_x \psi(0, \lambda) = 1$  and  $\partial_x \phi(0, \lambda) = \psi(0, \lambda) = 0$ , the monodromy matrix  $M_L$  is defined as

$$M_L(\lambda) := \begin{pmatrix} \phi(L, \lambda) & \psi(L, \lambda) \\ \partial_x \phi(L, \lambda) & \partial_x \psi(L, \lambda) \end{pmatrix}. \quad (3.3)$$

$M_L(\lambda)$  is a square matrix with determinant equal to 1, meaning that it can be viewed as a map  $M_L : \mathbb{R} \rightarrow \text{SL}(2, \mathbb{R})$ . The crucial information about the spectrum of  $\mathcal{H}_L$  is given by the eigenvalues of  $M_L$ , which are in turn determined by its trace. As a result, the trace of the monodromy matrix

$$\Delta_L(\lambda) := \text{tr } M_L(\lambda) = \phi(L, \lambda) + \partial_x \psi(L, \lambda), \quad (3.4)$$

will be the key quantity arising from the analysis of these operators. It is often known as the *discriminant* of the operator  $\mathcal{H}_L$ . Based on its trace, any matrix in  $\text{SL}(2, \mathbb{R})$  can be sorted into one of three categories:

- (i) If its trace is in  $(-\infty, -2) \cup (2, \infty)$ , then a matrix in  $\text{SL}(2, \mathbb{R})$  is said to be *hyperbolic* and it has two distinct real eigenvalues which satisfy  $\lambda_1 = \lambda_2^{-1}$ .
- (ii) If its trace is equal to  $\pm 2$ , then a matrix in  $\text{SL}(2, \mathbb{R})$  is said to be *parabolic* and it has a single real eigenvalue satisfying  $\lambda_1 = \pm 1$ .
- (iii) If its trace is in  $(-2, 2)$ , then a matrix in  $\text{SL}(2, \mathbb{R})$  is said to be *elliptic* and it has two complex eigenvalues which satisfy  $\lambda_1 = \lambda_2^*$  and  $|\lambda_1| = |\lambda_2| = 1$ .

The spectrum of the  $L$ -periodic operator  $\mathcal{H}_L$  has some convenient properties. In particular, it consists of a countable series of spectral “bands”, as specified by the following result, which can be found in [27, Theorem 1.12].

**Lemma 3.** *There exists a series of real numbers*

$$a_1 < b_1 \leq a_2 < b_2 \leq a_3 < \dots$$

*which are such that  $a_n, b_n \rightarrow \infty$  as  $n \rightarrow \infty$  and the spectrum  $\sigma(\mathcal{H}_L)$  is given by*

$$\sigma(\mathcal{H}_L) = \bigcup_{n=1}^{\infty} [a_n, b_n].$$



The nature of the eigenmodes within the spectral bands described in Lemma 3 can be illuminated through an application of *Floquet-Bloch theory*. That is, consider the eigenvalue problem (3.2) restricted to the subset

$$L_k^2 := \{u \in L_{\text{loc}}^2 : u(x+L) = e^{ikL}u(x)\}. \quad (3.5)$$

With this restriction, the eigenvalue problem is self adjoint so has a discrete, countable set of eigenvalues

$$\lambda_1(k) \leq \lambda_2(k) \leq \lambda_3(k) \leq \dots, \quad (3.6)$$

known as *band functions*. Each band function  $\lambda_j : \mathbb{R} \rightarrow \mathbb{R}$  is analytic and  $2\pi/L$ -periodic, meaning it will be sufficient to consider  $k$  in the set  $\mathcal{B} := [-\pi/L, \pi/L)$ , which is known as the *Brillouin zone*. Any solution to the eigenvalue problem (3.2) must be in  $L_k^2$  for some  $k$  in the Brillouin zone, meaning the entire spectrum is obtained through this approach [27, Theorem 1.14].

**Lemma 4.** *The spectrum  $\sigma(\mathcal{H}_L)$  is given by the union of all the band functions over all of the Brillouin zone:*

$$\sigma(\mathcal{H}_L) = \bigcup_{j=1}^{\infty} \bigcup_{k \in \mathcal{B}} \lambda_j(k).$$

The link between the monodromy matrix  $M_L$  and the Floquet-Bloch spectrum of  $\mathcal{H}_L$  arises through realising that if  $u \in L_k^2$  is a solution to  $\mathcal{H}_L u = \lambda u$ , then  $e^{ikL}$  must be an eigenvalue of  $M_L(\lambda)$ . This can be seen by an application of Floquet's Theorem (see *e.g.* [27, Theorem 1.3]) or by realising that  $M_L(\lambda)$  maps the solution and its derivative at  $x$  to the same quantities at  $x+L$  (see *e.g.* [9, Section 2.2]). Thus,  $\lambda \in \sigma(\mathcal{H}_L)$  if and only if there is some  $k \in \mathcal{B}$  such that

$$\det(M_L(\lambda) - e^{ikL}I) = 0. \quad (3.7)$$

The set of all  $(k, \lambda) \in \mathbb{R}^2$  satisfying this equation is known as the *dispersion relation*. Using the fact that  $\det(M_L) = 1$ , this is equivalent to

$$2 \cos(kL) = \Delta_L(\lambda). \quad (3.8)$$

The function  $k \mapsto \lambda$  is many valued and the branches are exactly the spectral band functions  $\lambda_j(k)$  from (3.6). From (3.8), it is clear that the band functions are even functions of  $k$ . Further, the band functions  $\lambda_j : \mathbb{R} \rightarrow \mathbb{R}$  are monotonic on each of the sets  $[-\pi, 0)$  and  $[0, \pi)$  (see also [33]). Finally, it is clear that (3.8) admits a real-valued solution  $\lambda(k)$  for real  $k$  if and only if  $|\Delta_L(\lambda)| \leq 2$ .

**Lemma 5.** *The spectrum  $\sigma(\mathcal{H}_L)$  is given by the values of  $\lambda \in \mathbb{R}$  such that  $\Delta_L(\lambda) \in [-2, 2]$ :*

$$\sigma(\mathcal{H}_L) = \{\lambda \in \mathbb{R} : |\Delta_L(\lambda)| \leq 2\}.$$

### 3.2. Density of states

The spectral theory of periodic elliptic operators not only reveals the nature of the spectrum  $\sigma(\mathcal{H}_L)$  (a countable series of spectral bands) but also some insight into how eigenstates are distributed within  $\sigma(\mathcal{H}_L)$ . In particular, it is possible to define a *density of states* which keeps track of where eigenstates occur within the spectral bands.

The typical (and most intuitive) way to introduce the density of states is by considering the restriction of the periodic operator  $\mathcal{H}_L$  to some domain  $[-R, R]$  and then letting  $R \rightarrow \infty$ . Appropriate boundary conditions need to be imposed at the edges of this domain: either periodic boundary conditions or Dirichlet boundary conditions are sufficient, for example. The restricted operator has a discrete spectrum so it makes sense to define the counting function  $\sum_{j=1}^{\infty} [\lambda_j < \lambda]$  which counts the number of eigenvalues less than  $\lambda$  (here,  $[\bullet]$  denotes the Iverson bracket, which takes the value 1 whenever the argument is true). The *integrated density of states* (often abbreviated to “IDS”) can subsequently be defined as the corresponding limit of the counting function:

$$\nu(\lambda) := \lim_{R \rightarrow \infty} \frac{1}{2R} \sum_{j=1}^{\infty} [\lambda_j < \lambda]. \quad (3.9)$$

The limit of the discrete spectrum has been studied in a variety of periodic systems with various boundary conditions [3, 6, 13, 14, 40]. For most reasonable choices of boundary conditions (such as either Dirichlet or Neumann boundary conditions), the limit in (3.9) exists (and is independent of the choice of boundary conditions) [2, 36].

The integrated density of states (3.9) can be re-cast in terms of the spectral band functions  $k \mapsto \lambda_j(k)$ , as in [27, Theorem 6.18].

**Lemma 6.** *The integrated density of states (3.9) is equal to*

$$\nu(\lambda) = \sum_{j=1}^{\infty} \mu\{k \in \mathcal{B} : \lambda_j(k) < \lambda\},$$

where  $\mu$  is the normalised Haar measure  $(2\pi)^{-1}dk$ .

From the analyticity of the band functions, it is immediately clear from Lemma 6 that the integrated density of states is also (piecewise) analytic. However, and this is crucial for this work, the integrated density of states can be singular at points where a band function  $k \mapsto \lambda_j(k)$  is at a critical value (or if it is singular, however that will not be the case for systems considered here). These singularities are known as *Van Hove singularities* [41].

While the integrated density of states is the most immediate notion of spectral density, it is often more informative to think about the *density of states* itself. This can be defined as the Radon–Nikodym derivative of the integrated density of states with respect to the Lebesgue measure:

$$D(\lambda) := \frac{d\nu}{d\lambda}. \quad (3.10)$$

Thanks to the characterisation of the integrated density of states in terms of the spectral band functions from Lemma 6, the density of states can also be reframed in terms of the spectral bands. Thanks to the one-dimensional nature of the Hill operators considered here, this takes amounts to summing the reciprocals of the slopes of the band functions over each level set.

**Lemma 7.** *The density of states  $D$  is equivalently given by*

$$D(\lambda) = \frac{1}{2\pi} \sum_{j=1}^{\infty} [\lambda_j = \lambda] \left| \frac{d\lambda_j}{dk} \right|^{-1},$$

where  $[\bullet]$  denotes the Iverson bracket, which takes the value 1 whenever the argument is true and 0 otherwise.

*Proof.* By computing the integral over the level set  $\lambda_j = \lambda$  in the definition of the integrated density of states (3.9), a formula for  $D$  can be obtained [27, Theorem 6.21]:

$$D(\lambda) = \frac{1}{2\pi} \sum_{j=1}^{\infty} \int_{\lambda_j=\lambda} \left| \frac{d\lambda_j}{dk} \right|^{-1} ds. \tag{3.11}$$

The one-dimensional nature of the problem (and the fact that the band functions are necessarily monotonic on each half of the Brillouin zone) means the level sets are just points, leading to the desired formula.  $\square$

From Lemma 7 it is apparent that Van Hove singularities will occur whenever a band function  $k \mapsto \lambda_j(k)$  has zero slope. In general, in this one-dimensional setting where the band functions are monotonic, this will happen at the edges of the reduced Brillouin zone. This can be seen by differentiating the dispersion relation (3.8) with respect to  $k$  to give

$$-2L \sin(kL) = \frac{d\Delta_L}{d\lambda} \frac{d\lambda}{dk}, \tag{3.12}$$

from which it is clear that  $d\lambda/dk = 0$  when  $k \in \{0, \pm\pi/L\}$  (provided the  $d\Delta_L/d\lambda$  is non-zero).

#### 4. Fibonacci tilings

Although the spectrum of a Hill operator  $\mathcal{H}_L$  (3.1) with  $L$ -periodic potential function  $V$  is always composed of a countable union of spectral bands (Lemma 3), this spectrum can be more or less intricate, depending on the choice of  $V$ . In particular, interesting behaviour can emerge by considering sequences of operators  $\mathcal{H}_{L_n}$  with associated potential functions  $V_n$  whose periodic unit cell becomes increasingly large (that is,  $L_n \rightarrow \infty$  as  $n \rightarrow \infty$ ). As the periodicity length  $L_n$  increases, the associated Brillouin zone  $\mathcal{B} = [-\pi/L_n, \pi/L_n)$  is correspondingly reduced in size and the number of disjoint spectral bands within each finite region of frequency space typically grows.

An example of a sequence of periodic materials that has received significant interest is the sequence of potential functions formed by a *Fibonacci tiling rule*. A Fibonacci tiling rule is an example of a two-letter substitution rule [15]. That is, given two letters  $A$  and  $B$ , a sequence of words can be formed by applying the substitution rule

$$A \rightarrow AB \quad \text{and} \quad B \rightarrow A. \quad (4.1)$$

Applying this rule to the starting value of  $\mathcal{F}_1 = A$  (or, equivalently,  $\mathcal{F}_0 = B$ ), gives the sequence of words

$$\begin{aligned} \mathcal{F}_0 &= B, \\ \mathcal{F}_1 &= A, \\ \mathcal{F}_2 &= AB, \\ \mathcal{F}_3 &= ABA, \\ \mathcal{F}_4 &= ABAAB, \\ \mathcal{F}_5 &= ABAABABA, \end{aligned} \quad (4.2)$$

and so on. This tiling rule is given the name ‘‘Fibonacci’’ since each word in (4.2) is given by combining the two previous words (*i.e.*  $\mathcal{F}_{n+1} = \mathcal{F}_n \cup \mathcal{F}_{n-1}$ ). As a result, the number of letters in each word follows the Fibonacci sequence ( $F_0 = 1$ ,  $F_1 = 1$ ,  $F_2 = 2$ ,  $F_3 = 3$ ,  $F_4 = 5$ ,  $F_5 = 8$ , and so on).

Given the sequence of Fibonacci tilings (4.2), periodic systems can be constructed. These are ‘‘two-phase’’ systems in the sense that they are composed of two distinct building blocks, which are assigned the labels  $A$  and  $B$ . Given a Fibonacci word  $\mathcal{F}_n$ , which contains  $F_n$  letters, the unit cell of the corresponding periodic system can be built by taking the  $F_n$  building blocks and arranging them according to the word. In the setting of the Hill operators considered here, it means that  $\mathcal{H}_{F_n}$  is the operator with potential  $V$  that is  $F_n$ -periodic. On its unit cell,  $V : [0, F_n) \rightarrow \mathbb{R}$  is given by

$$V(x) = \begin{cases} \alpha(x) & \text{for } m-1 \leq x < m \text{ if } \mathcal{F}_n[m] = A, \\ \beta(x) & \text{for } m-1 \leq x < m \text{ if } \mathcal{F}_n[m] = B, \end{cases} \quad (4.3)$$

where  $\mathcal{F}_n[m]$  is used to denote the  $m^{\text{th}}$  letter of the word  $\mathcal{F}_n$  and  $\alpha$  and  $\beta$  are some distinct piecewise smooth functions (in fact, in what follows they will be taken to be constant).

Recently, systems with structures based on Fibonacci tiling rules have been studied in many different settings [21]. This has included theoretical studies as well as experimental realisations of vibro-acoustic [12], photonic [42] and microwave [20] systems. Some exotic effects have been observed, such as negative refraction [31] and defect-induced localisation [9]. The spectral properties of the associated sequence of differential operators have also been studied. The limiting material is an example of a one-dimensional quasicrystal [26]. The sequence of spectral bands is known to converge to a Cantor set [24, 39] and contains large gaps that emerge early in the sequence and

are preserved throughout (coined *super band gaps*) [10, 32]. The integrated density of states for the sequence of periodic operators was studied by [29], who observed the expected self-similar properties and stable gaps.

The connection between periodic Hill operators generated by Fibonacci tilings and the non-linear recursion relation (1.1) is that the discriminants  $\Delta_{F_n}(\lambda)$  of the sequence of operators  $\mathcal{H}_{F_n}$  will satisfy (1.1). That is,

$$\Delta_{F_{n+1}}(\lambda) = \Delta_{F_n}(\lambda)\Delta_{F_{n-1}}(\lambda) - \Delta_{F_{n-2}}(\lambda), \quad (4.4)$$

for any  $\lambda \in \mathbb{R}$  and  $n \geq 2$ . This link was first discovered by [23] and is straightforward to show from the observation that successive monodromy matrices for periodic systems generated by a Fibonacci tiling are related by  $M_{F_n} = M_{F_{n-2}}M_{F_{n-1}}$ . Rearranging this to give  $M_{F_{n-2}}^{-1} = M_{F_{n-1}}M_{F_n}^{-1}$  and adding it to  $M_{F_{n+1}} = M_{F_{n-1}}M_{F_n}$  gives

$$M_{F_{n+1}} + M_{F_{n-2}}^{-1} = M_{F_{n-1}}M_{F_n} + M_{F_{n-1}}M_{F_n}^{-1}. \quad (4.5)$$

Taking the trace and using the fact that  $\text{tr}(M_{F_{n-1}}M_{F_n}) + \text{tr}(M_{F_{n-1}}M_{F_n}^{-1}) = \text{tr}(M_{F_{n-1}})\text{tr}(M_{F_n})$  gives (4.4).

The main idea in this work is to use this link with periodic Hill operators generated by Fibonacci tilings to predict the statistics of (1.1). That is, suppose an orbit of the recursion relation (1.1) has initial conditions  $x_0, x_1$  and  $x_2$ . If there exist distinct systems which can be assigned the labels  $A$  and  $B$  and are such that the discriminants of the resulting periodic operators based on Fibonacci tilings satisfy

$$\Delta_{F_0}(\lambda) = x_0, \quad \Delta_{F_1}(\lambda) = x_1 \quad \text{and} \quad \Delta_{F_2}(\lambda) = x_2, \quad (4.6)$$

then all subsequent elements of the sequence will satisfy  $x_n = \Delta_{F_n}(\lambda)$ . As a result, the density of states (3.10) can be used to predict how the values of  $x_n$  will be distributed.

Consider the setting where the constituent materials  $A$  and  $B$  are homogeneous. Thus, suppose that the potential  $V$  is piecewise constant and is given by (4.3) with  $\alpha, \beta \in \mathbb{R}$  being positive constant values with  $\alpha \neq \beta$ . Then, the monodromy matrices corresponding to  $\mathcal{F}_0 = B$  and  $\mathcal{F}_1 = A$  are given, respectively, by

$$M_{F_0} = \begin{pmatrix} \cos \omega_0 & \frac{1}{\omega_0} \sin \omega_0 \\ -\omega_0 \sin \omega_0 & \cos \omega_0 \end{pmatrix} \quad \text{and} \quad M_{F_1} = \begin{pmatrix} \cos \omega_1 & \frac{1}{\omega_1} \sin \omega_1 \\ -\omega_1 \sin \omega_1 & \cos \omega_1 \end{pmatrix}, \quad (4.7)$$

where  $\omega_0 = \sqrt{\beta - \lambda}$  and  $\omega_1 = \sqrt{\alpha - \lambda}$ . Hence, the associated discriminants are given by

$$\Delta_{F_0} = 2 \cos \omega_0 \quad \text{and} \quad \Delta_{F_1} = 2 \cos \omega_1. \quad (4.8)$$

The monodromy matrix  $M_{F_2}$  corresponding to  $\mathcal{F}_2 = AB$  is given by  $M_{F_2} = M_{F_0}M_{F_1}$ . Computing this matrix product and taking the trace of  $M_{F_2}$  gives the discriminant

$$\Delta_{F_2} = 2 \cos \omega_0 \cos \omega_1 - \left( \frac{\omega_0}{\omega_1} + \frac{\omega_1}{\omega_0} \right) \sin \omega_0 \sin \omega_1. \quad (4.9)$$

This is the formula that was specified in (2.5) and used to fix the dependence of  $x_2$  on  $x_1$  and  $x_0$ . Thus, by choosing this relationship between the initial values, it is guaranteed that  $x_2 = \Delta_{F_2}(\lambda)$ . As a result, (4.6) holds and there will be a correspondence between the orbit of the recursion relation and the sequence of Hill operators.

## 5. Main result

The main aim of this work is to use the link between the recursion relation (1.1) and periodic operators formed by Fibonacci tilings to predict the statistics of the recursion relation. In particular, the goal is to calculate the density of states  $D(x)$  of orbits of the recursion relation (1.1) restricted to the interval  $[-2, 2]$ . Thanks to the bijection with the discriminants of operators generated by a Fibonacci tiling rule, thanks to which it holds that  $x_n = \Delta_{F_n}$ , it will suffice to compute the density of states  $D(\Delta)$  for the discriminant.

The density of states  $D(\Delta)$  for the discriminant can be handled in the same way as in Section 3.2. The integrated density of states is defined using counting functions applied to the discrete spectra in the limit of increasingly large finite truncations of the domain:

$$\nu(\Delta) := \lim_{R \rightarrow \infty} \frac{1}{2R} \sum_{j=1}^{\infty} [\Delta_L(\lambda_j) < \Delta]. \quad (5.1)$$

Then, the density of states is, once again, given by the Radon–Nikodym derivative with respect to the Lebesgue measure:

$$D(\Delta) := \frac{d\nu}{d\Delta}. \quad (5.2)$$

The main result of this work is the following formula for  $D(\Delta)$ , which can be equivalently viewed as  $D(x)$ , the density of states of orbits of the recursion relation (1.1) restricted to the interval  $[-2, 2]$ .

**Theorem 8.** *The density of states  $D(x)$  of orbits of the recursion relation (1.1) restricted to the interval  $[-2, 2]$ , with initial conditions chosen such that  $x_0$  and  $x_1$  are independent uniform random variables on  $[-2, 2]$  and  $x_2$  satisfies (2.5), is given by*

$$D(x) = \frac{1}{\pi} \frac{1}{\sqrt{4 - x^2}},$$

for  $-2 < x < 2$ .

*Proof.* As discussed above, it is equivalent to calculate the density of states  $D(\Delta)$  for the discriminant, as defined in (5.2).

Following the arguments around Lemma 6, the integrated density of states  $\nu(\Delta)$  can be rewritten as

$$\nu(\Delta) = \sum_{j=1}^{\infty} \mu\{k \in \mathcal{B} : \Delta_L(\lambda_j(k)) < \Delta\}. \quad (5.3)$$

Given that the underlying Hill operators are one-dimensional, the band functions  $k \mapsto \lambda_j(k)$  are necessarily monotonic and the dispersion relation (3.8) gives that  $\Delta_L = 2 \cos kL$ . As a result, whenever  $\Delta_L$  is within the interval  $[-2, 2]$  it is a well-defined function of  $k \in \mathcal{B}$  and the dependence on  $\lambda_j$  in (5.3) can be dropped. Hence, (5.3) can be simplified to

$$\nu(\Delta) = \mu\{k \in \mathcal{B} : \Delta_L(k) < \Delta\}, \quad (5.4)$$

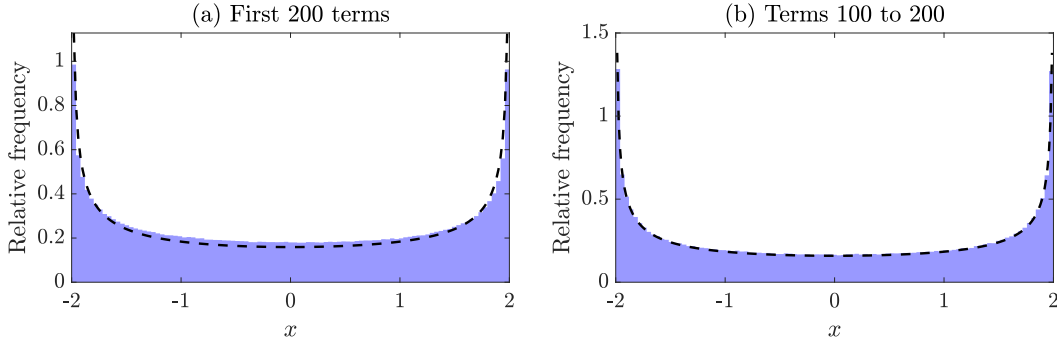


Figure 4: The long-time distribution of states of the recursion relation (1.1) when the initial values  $x_0$  and  $x_1$  are independent and uniformly distributed on  $[-2, 2]$  and  $x_2$  is chosen to depend on  $x_0$  and  $x_1$  according to (2.5). The histograms contain data from (a) the first 200 terms, *i.e.*  $\{x_0, x_1, \dots, x_{200}\}$ , and (b) terms in the interval 100 to 200, *i.e.*  $\{x_{100}, x_{101}, \dots, x_{200}\}$ . In both cases,  $10^5$  independent realisations of the initial conditions are used. The distribution from Theorem 8 is shown in a dashed line.

for  $-2 \leq \Delta \leq 2$ .

The density of states (5.2) can be calculated, using the same arguments as in Lemma 7, to be

$$D(\Delta) = \frac{d\nu}{d\Delta} = \frac{1}{2\pi} \left| \frac{d\Delta_L}{dk} \right|^{-1}. \quad (5.5)$$

Differentiating the dispersion relation  $\Delta_L = 2 \cos kL$  gives

$$\frac{d\Delta_L}{dk} = -2L \sin kL = -L\sqrt{4 - 4\cos^2 kL} = -L\sqrt{4 - \Delta_L^2}. \quad (5.6)$$

Substituting this into (5.5) and normalising so that  $\int_{-2}^2 D(\Delta) d\Delta = 1$  gives the desired formula for the density of states.  $\square$

The density of states  $D(x)$  obtained in Theorem 8 is compared to numerical data in Figure 4. The values of  $x_0$  and  $x_1$  are drawn independently from a uniform distribution on  $[-2, 2]$  and  $x_2$  is chosen to depend on  $x_0$  and  $x_1$  according to (2.5). This is repeated for  $10^5$  realisations and the first 200 terms of the recursion relation (1.1) are computed for each set of initial conditions. Figure 4(a) shows a histogram of all the values falling within the interval  $[-2, 2]$ . The density of states  $D(x)$  from Theorem 8 is shown with a dashed line and is seen to give a good prediction of the overall shape of the histogram. In particular, the clustering of values at the edges of the interval is well described by the Van Hove singularities in the density of states. However, there is a tendency for the calculated density of states  $D(x)$  to slightly underestimate in the centre of the interval and overestimate at the edges. This is due to the early terms in the orbits not following the calculated distribution (*e.g.*  $x_0$  and  $x_1$  are uniformly distributed and  $x_2$  follows the distribution described in Appendix B, by design). If the early terms are discarded, a closer agreement is observed. For example, in Figure 4(b) the first 100 terms are

discarded and only the terms  $\{x_{100}, x_{101}, \dots, x_{200}\}$  are shown in the histogram, leading to very close agreement between the numerical data and the theoretical density of states.

## 6. Concluding remarks

This work showed that constructing a sequence of periodic elliptic operators associated to a non-linear recursion relation provides an avenue for deriving an explicit formula for the long-time density of states. For the example studied here, this formula was shown to accurately predict the statistics from numerical experiments. It also revealed that the tendency for orbits of the non-linear recursion relation to cluster around the critical values  $x_n = \pm 2$  is connected to the Van Hove singularities in the density of states of the associated sequence of periodic elliptic operators.

A natural question to ask is whether appropriate sequences of operators could be constructed for other recursion relations. Firstly, this approach could be generalised straightforwardly to describe the behaviour of the same recursion relation (1.1) with different initial conditions (especially, different dependence of  $x_2$  on  $x_0$  and  $x_1$ ) by assigning different constituent “building blocks” to the labels  $A$  and  $B$  (rather than materials with constant potential). Secondly, the results could also be generalised easily to the non-linear recursion relations that are known to be associated to the *generalised* Fibonacci tiling rules. See [25] for details of these recursion relations, [16, 17, 18] for the basic spectral properties of the associated operators and [10] for analysis of the divergence of the associated recursion relations (equivalent “divergence horizon” results exist in many cases, with suitable growth criteria). Finally, generalising this work to an arbitrary non-linear recursion relation is a challenging open question. For example, the chaotic logistic map has a well-known invariant measure which describes the limiting distribution under uniform initial conditions and has similar singularities at the edges of the corresponding interval  $(0,1)$  [22, 35]. Are these singularities similarly related to the Van Hove singularities in the spectra of an associated sequence of periodic elliptic operators?

## Appendix A. Proof of Lemma 2

In this appendix, the probability density function  $f_{X_3}$  given in Lemma 2 is calculated, where  $X_3 = X_2X_1 - X_0$  with  $X_0$ ,  $X_1$  and  $X_2$  being independent and identically distributed random variables, drawn from uniform distributions on the interval  $[-2, 2]$ .

First, the density function of the product  $X_1X_2$  can be calculated using elementary properties of conditional probability. In particular, it holds for  $x \in [-2, 2]$  that

$$P(X_1X_2 \leq x) = \frac{1}{4} \int_{-2}^2 P(yX_2 \leq x) dy. \tag{A.1}$$

Solving this integral and then differentiating with respect to  $x$  gives that the probability



density function  $f_{X_2X_1}$  is given by

$$f_{X_2X_1}(x) = -\frac{1}{8} \log\left(\frac{|x|}{4}\right), \quad (\text{A.2})$$

for  $-4 \leq x \leq 4$  and vanishes outside of this interval.

Since  $X_2X_1$  and  $X_0$  are independent, the density function of their difference  $X_3 = X_2X_1 - X_0$  is given by the convolution of  $f_{X_2X_1}$  and  $f_{X_0}$ :

$$f_{X_3}(x) = \int_{-\infty}^{\infty} f_{X_2X_1}(x-z)f_{X_0}(z) dz = -\frac{1}{32} \int_{-2}^2 \log\left(\frac{|x-z|}{4}\right) \chi_{(-4,4)}(x-z) dz.$$

If  $x, z \in [-2, 2]$ , then  $|x-z| \leq 4$ , so  $\chi_{(-4,4)}(x-z) = 1$ . Thus, for  $-2 \leq x \leq 2$  it holds that

$$f_{X_3}(x) = -\frac{1}{32} \int_{-2}^2 \log\left(\frac{|x-z|}{4}\right) dz. \quad (\text{A.3})$$

Partitioning the integral into  $[-2, x]$  and  $[x, 2]$  gives

$$f_{X_3}(x) = -\frac{1}{32} \int_{-2}^x \log\left(\frac{x-z}{4}\right) dz - \frac{1}{32} \int_x^2 \log\left(\frac{z-x}{4}\right) dz, \quad (\text{A.4})$$

where each of the two integrals can be solved using integration by parts to obtain the formula stated in Lemma 2:

$$f_{X_3}(x) = \frac{x-2}{32} \log\left(\frac{2-x}{4}\right) - \frac{x+2}{32} \log\left(\frac{x+2}{4}\right) + \frac{1}{8}, \quad (\text{A.5})$$

for  $-2 \leq x \leq 2$ .

## Appendix B. Distribution of $x_2$

This appendix studies the distribution of the random variable  $X_2$ , given by

$$X_2 = 2 \cos \Omega_0 \cos \Omega_1 - \left(\frac{\Omega_0}{\Omega_1} + \frac{\Omega_1}{\Omega_0}\right) \sin \Omega_0 \sin \Omega_1, \quad (\text{B.1})$$

where  $\Omega_0$  and  $\Omega_1$  are given by

$$\Omega_0 = \arccos(X_0/2), \quad \Omega_1 = \arccos(X_1/2), \quad (\text{B.2})$$

with  $X_0$  and  $X_1$  being independent and identically distributed random variables, obeying uniform distributions on the interval  $[-2, 2]$ . It will not be possible to derive an explicit formula for the distribution of  $X_2$ , but the features of its distribution (shown in Figure B1(e)) can be better understood by examining each term in (B.1).

The first term of (B.1) can be understood easily, since  $2 \cos \Omega_0 \cos \Omega_1 = \frac{1}{2} X_0 X_1$ . Thus, it is possible to rescale the density function (A.2) to see that  $2 \cos \Omega_0 \cos \Omega_1$  has probability density function  $f_{2 \cos \Omega_0 \cos \Omega_1}$  given by

$$f_{2 \cos \Omega_0 \cos \Omega_1}(x) = -\frac{1}{4} \log\left(\frac{|x|}{2}\right), \quad (\text{B.3})$$

for  $-2 \leq x \leq 2$ , which vanishes outside of this interval. This distribution is shown in Figure B1(a), where the histogram shows  $10^6$  independent realisations of  $2 \cos \Omega_0 \cos \Omega_1$  and the dotted line shows the distribution (B.3).

To understand the second term of (B.1), the first step is to compute the distribution of  $\sin \Omega_0 \sin \Omega_1$ . If  $X_i$  is uniformly distributed on  $[-2, 2]$ , then  $\Omega_i = \arccos(X_i/2)$  has the probability density function

$$f_{\Omega_i}(\omega) = \frac{1}{2} \sin \omega, \quad (\text{B.4})$$

for  $0 \leq \omega \leq \pi$  and vanishes outside of this interval. Subsequently, the random variable  $\sin(\Omega_i)$  has the probability density function

$$f_{\sin(\Omega_i)}(y) = \tan(\arcsin y) = \frac{y}{\sqrt{1-y^2}}, \quad (\text{B.5})$$

for  $0 \leq y \leq 1$ , which vanishes outside of this interval. The product  $\sin \Omega_0 \sin \Omega_1$  can be handled by computing the cumulative distribution function

$$P(\sin \Omega_0 \sin \Omega_1 \leq x) = \int_0^1 P(y \sin \Omega_0 \leq x) \frac{y}{\sqrt{1-y^2}} dy. \quad (\text{B.6})$$

If  $x/y < 1$  then  $P(\sin \Omega_0 \leq x/y) = 1 - \sqrt{1-x^2/y^2}$ . Conversely, if  $x/y > 1$  then  $P(\sin \Omega_0 \leq x/y) = 1$ . Hence, the integral in (B.6) can be partitioned into the intervals  $[0, x]$  and  $[x, 1]$  to see that

$$P(\sin \Omega_0 \sin \Omega_1 \leq x) = 1 - \int_x^1 \frac{\sqrt{y^2 - x^2}}{\sqrt{1-y^2}} dy. \quad (\text{B.7})$$

To compute the density function, this expression should be differentiated with respect to  $x$ , for which the Leibniz integral rule can be used to see that

$$f_{\sin \Omega_0 \sin \Omega_1}(x) = \int_x^1 \frac{x}{\sqrt{y^2 - x^2} \sqrt{1-y^2}} dy. \quad (\text{B.8})$$

This integral can be expressed in terms of the complete elliptic integral of the first kind, which is the function  $K : (0, 1) \rightarrow \mathbb{R}$  defined as [1]

$$K(k) = \int_0^{\frac{\pi}{2}} \frac{1}{\sqrt{1 - k^2 \sin^2 t}} dt. \quad (\text{B.9})$$

Making an appropriate substitution and change of variables in the integral (B.8) gives that

$$f_{\sin \Omega_0 \sin \Omega_1}(x) = xK(1 - x^2). \quad (\text{B.10})$$

This distribution is shown in Figure B1(b), where the histogram shows  $10^6$  independent realisations of  $\sin \Omega_0 \sin \Omega_1$  and the dotted line shows the distribution (B.10).

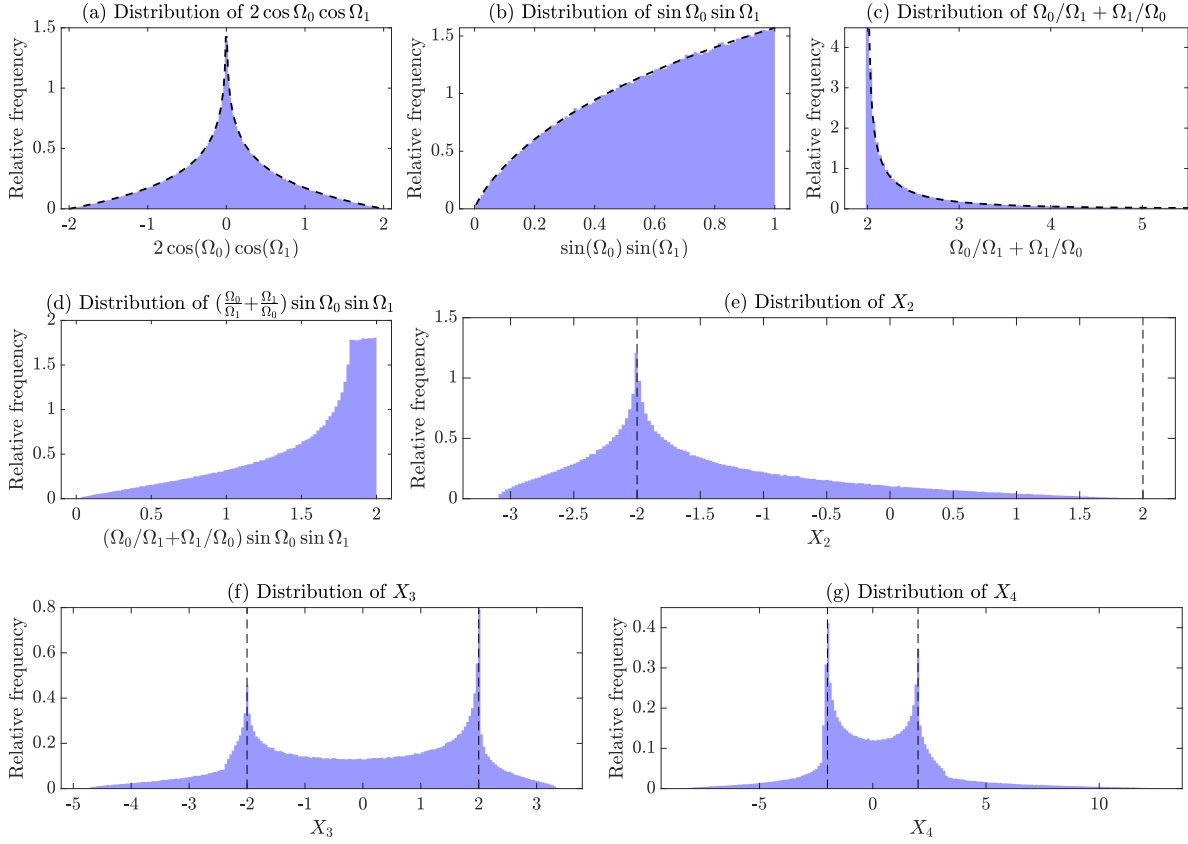


Figure B1: The distributions of the first few terms of the recursion relation (1.1) (and their key components). In (a), (b) and (c) the analytically computed distributions from (B.3), (B.10) and (B.20), respectively, are shown in dashed lines. In (e), (f) and (g) the critical thresholds  $\pm 2$  are marked by vertical dashed lines. In each case,  $10^5$  independent realisations of the initial conditions are used.

The missing piece needed to understand the distribution of  $X_2$  is the density function of  $\Omega_0/\Omega_1 + \Omega_1/\Omega_0$ . Given two independent random variables with density given by (B.4), their ratio has distribution

$$P\left(\frac{\Omega_0}{\Omega_1} \leq x\right) = \int_0^\pi P(\Omega_0 \leq xy) \frac{1}{2} \sin y \, dy, \quad (\text{B.11})$$

where  $x > 0$ . If  $0 < \pi/x < y$  then  $P(\Omega_0 \leq xy) = 1$ . Conversely if  $0 < y < \pi/x$  then

$$P(\Omega_0 \leq xy) = \int_0^{xy} \frac{1}{2} \sin t \, dt = \frac{1}{2} - \frac{1}{2} \cos xy. \quad (\text{B.12})$$

If  $x < 1$  then it must be the case that  $y < \pi < \pi/x$  so it can be calculated directly that

$$P\left(\frac{\Omega_0}{\Omega_1} \leq x\right) = \int_0^\pi \left(\frac{1}{2} - \frac{1}{2} \cos xy\right) \frac{1}{2} \sin y \, dy = \frac{1}{2} + \frac{1 + \cos \pi x}{4(x^2 - 1)}, \quad (\text{B.13})$$

which can be differentiated to find that  $\Omega_0/\Omega_1$  has probability density function given by

$$f_{\Omega_0/\Omega_1}(x) = -\frac{\pi(x^2 - 1) \sin \pi x + 2x(1 + \cos \pi x)}{4(x^2 - 1)^2}, \quad (\text{B.14})$$

for  $0 < x < 1$ . For  $x > 1$ , the integral in (B.11) can be handled by partitioning it into the intervals  $[0, \pi/x]$  and  $[\pi/x, \pi]$ :

$$\begin{aligned} P\left(\frac{\Omega_0}{\Omega_1} \leq x\right) &= \int_0^{\pi/x} \left(\frac{1}{2} - \frac{1}{2} \cos xy\right) \frac{1}{2} \sin y \, dy + \int_{\pi/x}^{\pi} \frac{1}{2} \sin y \, dy \\ &= \frac{3 + \cos \frac{\pi}{x}}{4} + \frac{1 + \cos \frac{\pi}{x}}{4(x^2 - 1)}, \end{aligned} \quad (\text{B.15})$$

which can be differentiated to obtain that

$$f_{\Omega_0/\Omega_1}(x) = \frac{\pi(x^2 - 1) \sin \frac{\pi}{x} - 2x(1 + \cos \frac{\pi}{x})}{4(x^2 - 1)^2}, \quad (\text{B.16})$$

for  $x > 1$ . Subsequently, the distribution of  $\Omega_0/\Omega_1 + \Omega_1/\Omega_0$  can be found by applying the transformation  $x \mapsto x + 1/x$ . This has a global minimum for  $x > 0$  at  $x = 1$  so it holds that

$$P\left(\frac{\Omega_0}{\Omega_1} + \frac{\Omega_1}{\Omega_0} \leq 2\right) = 0. \quad (\text{B.17})$$

Meanwhile, for any  $x \geq 2$ , it holds that

$$\begin{aligned} P\left(\frac{\Omega_0}{\Omega_1} + \frac{\Omega_1}{\Omega_0} \leq x\right) &= P\left(\frac{x - \sqrt{x^2 - 4}}{2} \leq \frac{\Omega_0}{\Omega_1} \leq \frac{x + \sqrt{x^2 - 4}}{2}\right) \\ &= P\left(\frac{\Omega_0}{\Omega_1} \leq \frac{x + \sqrt{x^2 - 4}}{2}\right) - P\left(\frac{\Omega_0}{\Omega_1} \leq \frac{x - \sqrt{x^2 - 4}}{2}\right). \end{aligned} \quad (\text{B.18})$$

Using (B.13) and (B.15), this becomes

$$\begin{aligned} P\left(\frac{\Omega_0}{\Omega_1} + \frac{\Omega_1}{\Omega_0} \leq x\right) &= \frac{1}{4} + \frac{1}{(x + \sqrt{x^2 - 4})^2 - 4} \left(1 + \cos\left(\frac{2\pi}{x + \sqrt{x^2 - 4}}\right)\right) \\ &+ \frac{1}{4} \cos\left(\frac{2\pi}{x + \sqrt{x^2 - 4}}\right) - \frac{1}{(x - \sqrt{x^2 - 4})^2 - 4} \left(1 + \cos\left(\frac{\pi}{2}(x - \sqrt{x^2 - 4})\right)\right) \end{aligned} \quad (\text{B.19})$$

which can be differentiated to obtain the probability density function

$$\begin{aligned} f_{\Omega_0/\Omega_1 + \Omega_1/\Omega_0}(x) &= \frac{1}{4(x^2 - 4)^{\frac{3}{2}}} \left[ -4 - 2 \cos\left(\frac{\pi}{2}(x - \sqrt{x^2 - 4})\right) \right. \\ &- 2 \cos\left(\frac{2\pi}{x + \sqrt{x^2 - 4}}\right) + \pi\sqrt{x^2 - 4} \sin\left(\frac{\pi}{2}(x - \sqrt{x^2 - 4})\right) \\ &\left. + \pi\sqrt{x^2 - 4} \sin\left(\frac{2\pi}{x + \sqrt{x^2 - 4}}\right) \right]. \end{aligned} \quad (\text{B.20})$$

This distribution is shown with the dashed line in Figure B1(c), where it is compared to a histogram showing  $10^6$  independent realisations of  $\Omega_0/\Omega_1 + \Omega_1/\Omega_0$ .

The distribution of  $X_2$  could now be obtained by a similar approach, however it is not reasonable to expect that explicit analytic expressions will be possible. Nevertheless, the density functions calculated above are already sufficient to yield some intuition on the qualitative properties of the distribution of  $X_2$ , which is shown in Figure B1(e).

First, consider the distribution of  $(\Omega_0/\Omega_1 + \Omega_1/\Omega_0) \sin \Omega_0 \sin \Omega_1$ . This variable must fall in the interval  $[0, 2]$  since it holds that  $0 \leq (x/y + y/x) \sin x \sin y \leq 2$  for  $0 \leq x, y \leq \pi$ . Further, this function attains its maximal value of 2 when  $x = y = \pi/2$ . Both  $\Omega_0$  and  $\Omega_1$  are drawn from distributions with sinusoidal density functions (B.4) which attain maxima at  $\pi/2$ . This explains why values tend to cluster around the upper end of the interval  $[0, 2]$ , as shown in Figure B1(d). The sharpness of this peak can be understood by examining the sharp peaks in the densities of  $\sin \Omega_i$  (B.5) and  $\Omega_0/\Omega_1 + \Omega_1/\Omega_0$  (B.20): the values of  $\sin \Omega_0$  and  $\sin \Omega_1$  are strongly clustered around 1 and the values of  $\Omega_0/\Omega_1 + \Omega_1/\Omega_0$  are strongly clustered around 2, leading to a peak in the density of their product close to 2.

The distribution of  $X_2$ , shown in Figure B1(e), is the difference between the distributions of  $2 \cos \Omega_0 \cos \Omega_1$  in Figure B1(a) and of  $(\Omega_0/\Omega_1 + \Omega_1/\Omega_0) \sin \Omega_0 \sin \Omega_1$  in Figure B1(d). In this case, there is strong clustering of values around -2. This can be understood from the fact that the density function of  $2 \cos \Omega_0 \cos \Omega_1$  in (B.3) has a singularity at 0 and the distribution of  $(\Omega_0/\Omega_1 + \Omega_1/\Omega_0) \sin \Omega_0 \sin \Omega_1$  in (B.20) shows clustering around 2. This clustering of values of  $X_2$  around -2 is the first hint of the Van Hove singularities studied in this work emerging. Examining the distributions of  $X_3$  and  $X_4$  in Figure B1(f) and Figure B1(g), the singularities around  $\pm 2$  are increasingly clear. As shown in Figure 4, as  $n$  becomes large the distribution of  $X_n$  confined to the interval  $[-2, 2]$  loses its asymmetry and the clustering of values around  $\pm 2$  converges to singularities in the density of states.

## Acknowledgements

This work was funded by the Engineering and Physical Sciences Research Council (EPSRC) through a fellowship with grant number EP/X027422/1. The author would like to thank Ian Hooper, whose comments were the inspiration for this work, as well as Matteo Tanzi for helpful discussions.

## Data availability

The software used to generate the numerical results presented in this article is available for download at <https://zenodo.org/doi/10.5281/zenodo.10986146>.

## References

- [1] M. Abramowitz and I. A. Stegun. *Handbook of Mathematical Functions with Formulas, Graphs, and Mathematical Tables*. Dover, New York, 1972.
- [2] T. Adachi and T. Sunada. Density of states in spectral geometry. *Comment. Math. Helvetici*, 68:480–493, 1993.
- [3] H. Ammari, B. Davies, and E. O. Hiltunen. Spectral convergence in large finite resonator arrays: the essential spectrum and band structure. *arXiv preprint arXiv:2305.16788*, 2023.
- [4] A. Avila and S. Jitomirskaya. The ten martini problem. *Ann. Math.*, 170(1):303–342, 2009.

- [5] R. E. Borland. The nature of the electronic states in disordered one-dimensional systems. *Proc. R. Soc. A*, 274(1359):529–545, 1963.
- [6] A. Bourget and T. Goode. Density of states of Jacobi matrices with periodic and asymptotically periodic coefficients. *Proc. Am. Math. Soc.*, 143(12):5293–5306, 2015.
- [7] R. Carmona. Exponential localization in one dimensional disordered systems. *Duke Math. J.*, 49(1):191–213, 1982.
- [8] A. Comtet, C. Texier, and Y. Tourigny. Lyapunov exponents, one-dimensional Anderson localization and products of random matrices. *J. Phys. A: Math. Theor.*, 46(25):254003, 2013.
- [9] B. Davies and R. V. Craster. Symmetry-induced quasicrystalline waveguides. *Wave Motion*, 115:103068, 2022.
- [10] B. Davies and L. Morini. Super band gaps and periodic approximants of generalised Fibonacci tilings. *Proc. R. Soc. A*, 480(2285):20230663, 2024.
- [11] L. Erdős and H.-T. Yau. *A Dynamical Approach to Random Matrix Theory*, volume 28 of *Courant Lecture Notes*. American Mathematical Society, 2017.
- [12] M. Gei, Z. Chen, F. Bosi, and L. Morini. Phononic canonical quasicrystalline waveguides. *Appl. Phys. Lett.*, 116(24), 2020.
- [13] J. S. Geronimo, E. M. Harrell, and W. Van Assche. On the asymptotic distribution of eigenvalues of banded matrices. *Constr. Approx.*, 4:403–417, 1988.
- [14] R. Gray. On the asymptotic eigenvalue distribution of Toeplitz matrices. *IEEE T. Inform. Theory*, 18(6):725–730, 1972.
- [15] B. Grünbaum and G. C. Shephard. *Tilings and Patterns*. Freeman, New York, 1986.
- [16] G. Gumbs and M. K. Ali. Dynamical maps, Cantor spectra, and localization for Fibonacci and related quasiperiodic lattices. *Phys. Rev. Lett.*, 60(11):1081, 1988.
- [17] G. Gumbs and M. K. Ali. Scaling and eigenstates for a class of one-dimensional quasiperiodic lattices. *J. Phys. A*, 21(9):L517, 1988.
- [18] G. Gumbs and M. K. Ali. Electronic properties of the tight-binding Fibonacci Hamiltonian. *J. Phys. A*, 22(8):951, 1989.
- [19] F. Haake. Quantum signatures of chaos. In B. Kramer, editor, *Quantum Coherence in Mesoscopic Systems*, volume 254 of *NATO ASI Series*. Springer, Boston, MA, 1991.
- [20] J. K. Hamilton, M. Camacho, R. R. Boix, I. R. Hooper, and C. R. Lawrence. Effective-periodicity effects in Fibonacci slot arrays. *Phys. Rev. B*, 104(24):L241412, 2021.
- [21] A. Jagannathan. The Fibonacci quasicrystal: Case study of hidden dimensions and multifractality. *Rev. Mod. Phys.*, 93(4):045001, 2021.
- [22] M. V. Jakobson. Absolutely continuous invariant measures for one-parameter families of one-dimensional maps. *Commun. Math. Phys.*, 81:39–88, 1981.
- [23] M. Kohmoto, L. P. Kadanoff, and C. Tang. Localization problem in one dimension: Mapping and escape. *Phys. Rev. Lett.*, 50(23):1870, 1983.
- [24] M. Kohmoto and Y. Oono. Cantor spectrum for an almost periodic Schrödinger equation and a dynamical map. *Phys. Lett. A*, 102(4):145–148, 1984.
- [25] M. Kolář and M. Ali. One-dimensional generalized Fibonacci tilings. *Phys. Rev. B*, 41(10):7108, 1990.
- [26] M. Kolář. New class of one-dimensional quasicrystals. *Phys. Rev. B*, 47(9):5489, 1993.
- [27] P. Kuchment. An overview of periodic elliptic operators. *Bull. Am. Math. Soc.*, 53(3):343–414, 2016.
- [28] A. Lasota and M. C. Mackey. *Chaos, Fractals, and Noise: Stochastic Aspects of Dynamics*, volume 97 of *Applied Mathematical Sciences*. Springer Science & Business Media, 2013.
- [29] J. M. Luck and D. Petritis. Phonon spectra in one-dimensional quasicrystals. *J. Stat. Phys.*, 42:289–310, 1986.
- [30] B. B. Mandelbrot. *Fractals and Chaos: The Mandelbrot Set and Beyond*. Springer, New York, 2004.
- [31] L. Morini, Y. Eyzat, and M. Gei. Negative refraction in quasicrystalline multilayered

- metamaterials. *J. Mech. Phys. Solids*, 124:282–298, 2019.
- [32] L. Morini and M. Gei. Waves in one-dimensional quasicrystalline structures: dynamical trace mapping, scaling and self-similarity of the spectrum. *J. Mech. Phys. Solids*, 119:83–103, 2018.
- [33] M. Reed and B. Simon. *Methods of Modern Mathematical Physics IV: Analysis of Operators*, volume 4. Elsevier, 1978.
- [34] J. A. Scales and E. S. Van Vleck. Lyapunov exponents and localization in randomly layered media. *J. Comput. Phys.*, 133(1):27–42, 1997.
- [35] J. P. Sethna. *Statistical Mechanics: Entropy, Order Parameters, and Complexity*. Oxford University Press, 2006.
- [36] M. A. Shubin. The spectral theory and the index of elliptic operators with almost periodic coefficients. *Russ. Math. Surv.*, 34(2):109, 1979.
- [37] B. Simon. Almost periodic Schrödinger operators: a review. *Adv. Appl. Math.*, 3(4):463–490, 1982.
- [38] S. Surace. The Schrödinger equation with a quasi-periodic potential. *Trans. Amer. Math. Soc.*, 320(1):321–370, 1990.
- [39] A. Sütő. Singular continuous spectrum on a Cantor set of zero Lebesgue measure for the Fibonacci Hamiltonian. *J. Stat. Phys.*, 56:525–531, 1989.
- [40] P. Tilli. On the asymptotic spectrum of Hermitian block Toeplitz matrices with Toeplitz blocks. *Math. Comput.*, 66(219):1147–1159, 1997.
- [41] L. Van Hove. The occurrence of singularities in the elastic frequency distribution of a crystal. *Phys. Rev.*, 89(6):1189, 1953.
- [42] M. Verbin, O. Zilberberg, Y. Lahini, Y. E. Kraus, and Y. Silberberg. Topological pumping over a photonic Fibonacci quasicrystal. *Phys. Rev. B*, 91(6):064201, 2015.
- [43] P. Walters. *An Introduction to Ergodic Theory*, volume 79 of *Graduate Texts in Mathematics*. Springer Science & Business Media, 2000.